EXPERIMENTAL STUDY OF TURBULENT STRUCTURES IN A NON ISOTHERMAL HORIZONTAL JET ISSUING FROM A ROUND NOZZLE MOVED FROM A WALL

Frédéric Kuznik[1*], Gilles Rusaouen[1], Jean Brau[1]
[1]CETHIL, CNRS, UMR 5008,
Bât. Sadi Carnot, 9 rue de la Physique, FR-69621, Villeurbanne
INSA-Lyon
Université de Lyon
[*]Correspondent author: Fax: +33-472-438-522 Email: frederic.kuznik@insa-lyon.fr

ABSTRACT

An non isothermal horizontal issuing from a round nozzle moved from a wall is investigated experimentally. We consider four cases: an isothermal jet, a hot air jet, a cold air jet interacting with the wall and a cold air jet falling down without reaching the wall. The jet expansion rates shows two categories: the isothermal jet and cold jet not adhering to the wall , with a vertical expansion rate higher than the lateral one and the non isothermal jets adhering to the wall, with a lateral expansion rate higher than the vertical one. The turbulence structures analysis confirms the two categories: the first one create highly anisotropic structures mainly cigar axisymmetric, the second one is subject to instabilities link to lateral air ejections. This is confirm by a spectral analysis of the turbulent component of the flow and a scenario of coherent structures evolution is proposed.

Key words: wall jet, buoyancy force, Lumley triangle, turbulence anisotropy, coherent structures, spectral analysis.

1. INTRODUCTION

The study of the flow due to a round jet exiting over a wall parallel to the jet axis is interesting for practical applications like ventilation (building applications for example) or film cooling. However, the case of the non isothermal flow is few studied, especially for low velocity jets where buoyancy effect plays an important role. Moreover, numerical predictions of such flows is only possible if the turbulent structures are known.

For three dimensional wall jet, the lateral growth rate is much higher than the normal growth rate perpendicular to the wall. Launder and Rodi (1983) supposed, by examining the governing equations for the mean streamwise vorticity, that there must be two regions of counter rotating mean streamwise vorticity on each side of the jet centerline. These regions were located one above the other so they acted to drive the fluid into the jet along the centerline and pump the fluid laterally out of the side of the jet, increasing the lateral spread rate of the jet.

Concerning the round wall jet, Matsuda et al. (1990) showed that the mean streamwise vorticity was not caused by steady secondary motion in the jet but were instead caused by large-scale structures formed in the near field of the jet. They proposed that the vortex ring structures shed by the jet and the wall caused the ring structures to incline forward so that the upper portion formed a large scale horseshoe vortex. Their measurements only concern the near field of the flow, 1.75 to 3 diameters downstream of the jet exit.

Ewing and Pollard (1997) extended Matsuda and al. investigations to the intermediate region of the jet, 3 to 10 diameters downstream of the jet exit. The jet studied was flush mounted onto a large base wall, the experimental set-up also including a large backing plate normal to the base wall. Their measurements suggest that the bottom region of the vortex ring were convected faster than the outer edges, forming an inner horseshoe vortices near the wall. This process is shown figure 1. The periodic lateral jet ejection is then caused by the horseshoe leg vortex, explaining the large lateral spread rate of the jet. Their experiments were conducted with a Reynolds number based on the exit diameter of 25000.

[Fig. 1 about here.]

The objective of this study is first to extend the study of round jet expansion to the case of the nozzle moved from the wall. The second objective is to investigate the case of the jet blown with a temperature different compare to the ambiant air temperature. The main interest is the turbulent structures of these fluid flows. The study concern the three zones of the jet flow(near exit zone, axisymmetric zone and terminal zone), 0.25 to 16 downstream of the jet exit.

2. EXPERIMENTAL SET-UP

The jet exited a contraction with an exit diameter of D = 0.12m. The air flow was provided by an air treatment system allowing us to regulate the airflow and the air temperature. The flow was conditioned using a settling chamber located before the contraction. The velocity profile at the jet exit was uniform to within 5% and the turbulence intensity was less than 10%.

The nozzle was mounted moved from a horizontal wall that had a width of 3.10m and a length of 3.10m. The distance of the horizontal wall to the center of the nozzle, H, was H/D = 1.5. The facility included a vertical backplane with a height of 1m mounted behind the nozzle to block entrainment of the air.

[Fig. 2 about here.]

The experimental apparatus was enclosed so that it forms an experimental test room. The complete test room diagram is shown figure 2. The external faces of the experimental test room were maintained at a constant temperature using a thermal guard. Thermocouples allowed us to verify that the thermal conditions did not changed during a complete set of measurements. The gravity direction is opposite to the z direction.

A mobile arm allowed to move a set of probes in the whole measurement volume. The probes were of two types: temperature probes and velocity probe. The mean temperature was measured using Pt100 sensor, calibrated with a resolution of ±0.2◦C. Three temperature probes were posted, on the mobile arm, along a vertical line. The three components of the instantaneous velocity were measured via a three hot-wires probe. This probe has been calibrated insitu along the three directions of the flow, taking into account the temperature of the fluid using a correlation developed by Kuznik (2005). The final calibration of the velocity probe was given with an uncertainty on the mean velocity measurement of ±0.05m/s. Only velocities which magnitude was higher than 0.1m/s were measurable by our means.

For a given position of the mobile arm, the quantities measured were the mean temperatures and 150000 samples of the three component of the velocity. Concerning the velocity, the sampling frequency were 5000Hz in order to avoid important uncertainties in the calculation of power spectral density (Van Dijk (1999)).

The non-dimensional parameters governing such flows are the initial Reynolds number and the Archimede number, both based on the exit diameter D, which definitions are:

$$\mathrm{Re}_{0,D} = \frac{U_0 D}{\nu}$$

$$Ar_{0,D} = \frac{g\beta\left(T_0 - T_m\right)D}{U_0^2}$$

where U_0 and T_0 are the mean velocity magnitude and temperature at the air exit, T_m the mean air temperature of the non moving fluid zone, ν the kinematic viscosity and β the coefficient of thermal expansion. The Archimede number characterize the initial buoyancy force compare with the initial inertial force.

The whole of the cases tested covered Reynolds numbers, based on the exit diameter, from 10400 to 23680 and Archimede number, based on the exit diameter, from -0.0145 to 0.017. Only 4 cases are presented in this article, but the conclusions and observations apply to all the cases tested. The table 1 presents the characteristics of the cases detailed in this paper: an isothermal case named I (the temperature of the air jet was equal to the mean temperature in the test room), a hot case named H (the temperature of the air jet was higher than the mean temperature in the test room), two cold cases C1 and C2 (the temperature of the air jet was lower than the mean temperature in the test room).

[Table 1 about here.]

3. MEAN FLOW RESULTS

The coordinates associated with the jet flow are shown figure 4. The values of x and y were normalized using the exit diameter D while the vertical coordinate z was normalized using the distance of the center of the nozzle to the wall named H. The measurements have been made in the median plan $x = 0$ and in several vertical plans $y = constant$.

3.1. Mean velocity vector field in the median plan

The mean velocity vector field are presented figure 3 in the median in order to understand the global behavior of each flow. It must be emphasized that the symmetry of the mean velocity field with respect to the median plan has been verified for all the cases tested.

[Fig. 3 about here.]

When the temperature of inflow is equal to the ambiant temperature, case I figure 3, the jet adheres to the wall due to both the natural expansion of the jet and the Coanda effect (the flow hit the wall at about $y/D = 6$). Along the y axis, the position of the mean velocity magnitude maximum move away from the wall, as it is has been reported in Benaissa et al. (2004). This effect is mainly due to the entrainment of the non-moving fluid zone which is under the jet.

Because of the buoyancy force, the hot jet shown figure 3 reaches the wall faster than for the isothermal case, at about $y/D = 45$. The more the fluid is far from the nozzle, the more the force due to the density differences surpasses the inertial force.

When the temperature of the inflow is lower than the ambiant temperature, the jet is falling due to the Archimede effect. The case C1, shown figure 3, is a jet which is reaching the wall before going down (the jet hits the wall at about $y/D = 6$); the case C2 is a jet which is falling without interacting with the wall.

3.2. Jet expansion rates

The parameters associated with the jet expansion rates are defined figure 4. Considering the mean velocity magnitude maximum U_m in a given section y and the half of its value $U_m/2$, $z_{0.5Um}$ is the distance along z between the position of U_m and $U_m/2$ and $x_{0.5Um}$ is the distance along x between the position of U_m and $U_m/2$. The lateral jet expansion rate α_l and the vertical jet expansion rate α_v are then given by:

$$\alpha_l = \frac{\partial x_{0.5Um}}{\partial y}$$

$$\alpha_v = \frac{\partial z_{0.5Um}}{\partial y}$$

In the case of a free isothermal jet, a literature review found in Chassaing (2000) gave the value of 0.091±0.01 for the expansion rate following a direction perpendicular to the jet axis.

[Fig. 4 about here.]

The expansion rates of all the cases tested are presented table 2. These results show that the jets can be classified into two different categories. The first one is composed of the isothermal jets and the cold jets which are going down without reaching the wall. These jets are characterized by a vertical jet expansion rate higher than the lateral one. Considering the second category, which is the non isothermal jets adhering to the wall, it is characterized by a lateral jet expansion rate higher than the lateral one.

[Table 2 about here.]

The three-dimensional wall jet behavior is mainly due to the turbulent structures present in the flow. Then, in order to explain the two different categories of flows found here, a turbulent analysis is necessary: that is the subject of the next section of this article.

4. TURBULENCE STRUCTURE ANALYSIS: THE LUMLEY TRIANGLE

4.1. Presentation

The Reynolds-stress tensor $R_{ij} = \overline{u_i' u_j'}$ being symmetric, it has orthogonal eigenvectors with real eigenvalues. The three eigenvalues are turbulent energies associated with turbulent motions in the direction of the respective eigenvectors.

The original Lumley triangle (Lumley (1978)) allows to characterize the anisotropy or R_{ij} .

However, a modified version of the original Lumley triangle developed by Pope (2000) is used because it provide a linear departure of the turbulence from the isotropic distribution.

The anisotropy tensor b_{ij} is defined by:

$$b_{ij} = \frac{R_{ij}}{2k} - \frac{1}{3}\delta_{ij}$$

with k the turbulent kinetic energy.

As the anisotropy tensor has zero trace, it has just two independent invariants II and III (the invariant $I = 0$) defined by:

$$II = -\frac{1}{2} b_{ij} b_{ij}$$

$$III = \frac{1}{3} b_{ip} b_{pj} b_{ji}$$

These invariants II and III are the original Lumley triangle coordinates. To linearise the Lumley diagram, it is convenient to take the two independent quantities II^* and III^* defined by:

$$II^* = 3\sqrt{-II}$$

$$III^* = 6\sqrt[3]{\frac{III}{2}}$$

[Table 3 about here.]

[Fig. 5 about here.]

At any point in any turbulent flow, II^* and III^* can be determined from the Reynolds stresses, and the result plotted as a point on the $II^* - III^*$ plane. There are some special states of the Reynolds-stress tensor that correspond to particular points and curves in this plane. These states are summarized in table 3 and plotted in figure 5.

Every Reynolds stress that occur in a turbulent flow correspond to a point inside the Lumley triangle. Point outside correspond to non-realizable Reynolds stresses.

Also shown in figure 5 are values obtained for the turbulent free isothermal jet, in the axisymmetric zone of the jet. While axisymmetric cigar turbulence occurs in the center zone of the jet, the outer part of the jet is mainly composed of axisymmetric pancake turbulence corresponding to the instability rings.

[Fig. 6 about here.]

4.2. Experimental results

In order to have a complete description of the turbulence in the flow, the measurement points in the median plan have been chose for the Lumley triangle analysis. The Lumley triangles for all the cases tested are presented figure 6.

The isothermal jet produces mainly cigar-axisymmetric turbulent structures. The figure 7 presents the directions of the eigenvectors associated to the highest eigenvalues of the Reynolds-stress tensor. The directions of the high-energy turbulent structures belong to the median plan. Some pancake structures, appearing near the jet exit, are due to the vortex ring. Then, the main difference between the wall jet and our configuration is that the primary vortex ring of the jet are not energetic enough to live until the horizontal wall. Moreover, The more the fluid moves away from the jet exit, the more the turbulent structures of the flow are anisotropic.

The turbulent structures in the hot jet flow are a mixing between cigar and pancake structures. There is no clear boundaries between cigar structures zone and pancake structures zone. In order to analyze these structures, the figure 8 displays the directions of the eigenvectors associated to the highest eigenvalues and the second highest eigenvalues of the Reynolds-stress tensor. High-energy turbulent structures occur perpendicularly to the median plan, explaining the pancake turbulence found with the help of the Lumley triangle. The turbulent flow perpendicular to the median plan exists everywhere in the jet.

The Lumley triangle of the cold jet reaching the wall is similar to the hot case one: a mixing between cigar and pancake turbulence structures. High-energy turbulent structures occur perpendicularly to the median plan, as it is shown figure 9. Concerning the turbulence structures, the hot jet (which adheres to the wall because of the buoyancy force) and the cold jet adhering to the wall are very close.

The cold jet which is not adhering to the wall is mainly composed of cigar structures of to types: axisymmetric and two-component. In the two cases, the turbulence is highly anisotropic and tend to be one-component as the flows evolve far from the jet exit. The figure 10 shows that two-component structures occur mainly from

y/D = 10, in the zone of the jet opposite to the wall (*z/H > 4*).

4.3. Conclusions

The analysis of the jet expansion rates allowed to distinguish to types of jets: on one hand, the isothermal jets and cold jets which are not adhering to the wall and on the other hand, the non isothermal jets adhering to the wall. The turbulent structures analysis confirms these two categories. The isothermal jets and col jets not adhering to the wall are manly composed of cigar turbulent structures which are highly anisotropic. The non isothermal jets adhering to the wall are composed of a mixed between cigar and pancake turbulent structures.

For the non isothermal jets adhering to the wall, high-energy turbulent structures occur perpendicularly to the median plan, explaining that the lateral expansion rate is higher than the vertical one. In order to investigate the source of these lateral structures, the next section of this article is dedicated to a spectral analysis of the flow.

[Fig. 7 about here.]

[Fig. 8 about here.]

[Fig. 9 about here.]

[Fig. 10 about here.]

5. TURBULENCE SPECTRAL ANALYSIS

5.1. Experimental results

For round wall jet, it is well known that periodic structures occur ejecting the flow laterally, signatures of which are identified by the streamwise velocity fluctuations (Matsuda et al. (1990)). Following the turbulence structures analysis, it can be expected that a similar feature exist in the present jet.

In order to check this feature, we measured the power spectral densities of velocity fluctuations *u'*, *v'* and *w'*. Each case is characterized by four measurement points which positions on *y* axis are *y/D = 0.67* (near the jet exit), *y/D = 3.58*, *y/D = 8.16* and *y/D = 14.42* (terminal zone of the jet). The vertical position (*z*) corresponds to the maximum velocity magnitude which is the optimal position for capturing the signatures of structures in the free jet case (Bruun (1977)). The figure 11 summarizes the results found for the power spectral densities, with arbitrary units, and for the four cases described previously.

While the isothermal jet and cold jet not adhering to the wall present a power spectral density decreasing when the frequency is increasing, the non isothermal jets adhering to the wall show a spectrum dominated by a discrete frequency peak of large magnitude (f_0) and its harmonics. These peaks occur from the near the jet exit to the terminal zone of the jet flow.The most energetic component of the flow is *u'*, which is perpendicular to the median plan, confirming the results of the turbulence structures analysis.

The characteristic frequency of the peaks f_0 is defined as the most energetic

frequency. Following this definition, $f_0 = 48Hz$ for the non isothermal jets adhering to the wall; this frequency did not depend on the Reynolds number and the Archimede number for all the cases tested. The Strouhal number (f_0D/U_0) is about 3.6.

[Fig. 11 about here.]

5.2. Conclusions

It has been shown that lateral ejections occur in the case of non isothermal jets adhering to the wall, with consequences a large lateral growth rate comparing to the vertical one and a mixed between pancake and cigar turbulent structures in the flow.

The observation that the power spectral density is dominated by a discrete frequency peak of large magnitude and its higher harmonics suggests the occurrence of a new phenomenon. The time records used for calculating these spectra are so long that many wave crest pass by the fixed hot-wire position during a single time record. In order to produce such spiky spectra, there must be relatively random variation from one passing structure to the next: coherent structures exists and the following scenario is proposed.

The primary jet instability, composed of vortex rings, is a Kelvin-Helmhotz instability due to the velocity difference between the jet and the non-moving fluid zone. For the non isothermal flow, the density difference between the jet and the non-moving fluid zone combine with the

velocity difference to produce the Kelvin-Helmhotz instability. The gravity effect is to stabilize the low frequency instability and destabilize the high frequency instability. The primary vortex ring, which are low frequency, are then stabilize and can live until the wall. The vortex ring arriving at the wall then follow the scenario proposed by Ewing and Pollard (1997) shown figure 1 and horseshoe vortex produce lateral ejections. The primary vortex ring are then slow down by the horseshoe vortex, and the occurrence of a vortex pairing is suggested to explain that the instabilities exist from the air jet exit to the terminal zone of the jet.

6. CONCLUSIONS

This experimental exploration of the horizontal non isothermal jet issuing form a round nozzle moved from a wall settled physical issues concerning the turbulent structures occurring in such flows. Two different categories of jet can be found:on one hand, the isothermal jets and cold jet which are not adhering to the wall and and the other hand, the non isothermal jet adhering to the wall. From a mean flow point of view, the first category of jets has a vertical growth rate higher than the lateral one whereas the second type of jets is characterized by a lateral expansion rate higher than the vertical one, as for standard three-dimensional wall jet.

The characterization of turbulent structures occurring in the different flows is a challenge for a better understanding of the jets behavior and can provide tools for numerical simulations by computational fluid dynamics (CFD). The isothermal jets and cold jets not adhering to the wall developed turbulent structures highly anisotropic and mainly axisymmetric. For the CFD simulations, using two equations closure turbulence models is then inappropriate because of their impossibility to predict anisotropy (which is confirm by the results of Kuznik et al. (2005)).

Concerning the non isothermal jets adhering to the wall, they are subject to instabilities producing lateral ejections. The turbulence is then composed of a mixed between pancake and cigar structures. The primary vortex rings of the jet first combine with the wall to produce horseshoe structures which eject the fluid in the orthogonal direction according to the symmetry plan of the jet. As the horseshoe structures are slowed down by the wall, the vortex ring upstream these coherent structures the vortex ring can pairing and eject the fluid laterally. Of course, this is just a proposed scenario of coherent structures evolution, and it has to be verify experimentally. The CFD modelling of such flows need at least large eddy simulation turbulence models.

REFERENCES

Benaissa, A., Fleck, B.A. and Pollard, A. 2004. Wall effects on an axisymetric jet evolution. International Journal of Transport Phenomena 6, 323–331.

Bruun, H.H. 1977. A time-dmain analysis of large-sclae flow structure in a circular jet. Journal of Fluid Mechanics 83, 641–671.

Chassaing, P. 2000. Turbulence en m´ecanique des fluides. Toulouse POLYTECH Press.

Ewing, D. and Pollard, A. 1997. Evolution of the large scale motions in a three dimensionnal wall jet. AIAA-97-1964.

Hussein, H.J., Capp, S. and George, W.K. 1994. Velocity measurement in a high-reynolds-number, momentum-conserving, axisymetric, turbulent jet. Journal of Fluid Mechanics 258, 31–75.

Kuznik, F. 2005. Etude expérimentale des jets axisymétriques anisothermes horizontaux se développant près d'une paroi - Application à la modélisation numérique des cavités ventilées. Ph. D. Thesis, INSA de Lyon.

Kuznik, F., Rusaouen, G. and Hohota, R. 2005. Comparisons of two equations turbulence models for the prediction of heat and mass transfer in a mechanically ventilated anclosure. Proceeding of Fourth International Conference on Computational Heat and Mass Transfer, Paris 17-20 May 2005.

Lumley, J.L. 1978. Computational modeling of turbulent flows. Advances in Applied Mechanics 18, 123–176.

Launder, B.E. and Rodi, W. 1983. The turbulent wall jet - Measurement and modeling. Ann. Rev. of Fluid. Mech. 15, 429–459.

Mastuda, H., Iida, S. and Hayakawa, M. 1990. Coherent structures in a three dimensionnal wall jet. Journal of Fluid Engineering 112, 462–467.

Pope, S.B. 2000. Turbulent flows. Cambridge University Press.

Van Dijk, A. 1999. Aliasing in one-point turbulence measurements. Ph. D. Thesis, Delft Technical University.

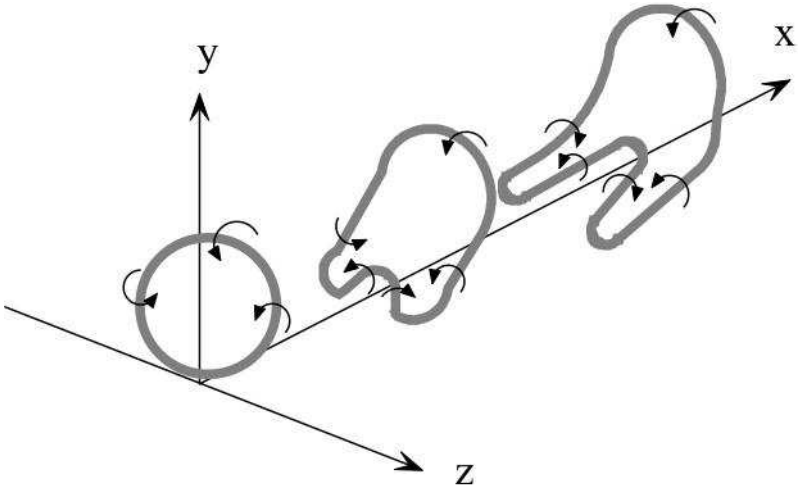

Figure 1 Model evolution of the large-scale structures in the jet proposed by Ewing and Pollard (1997)

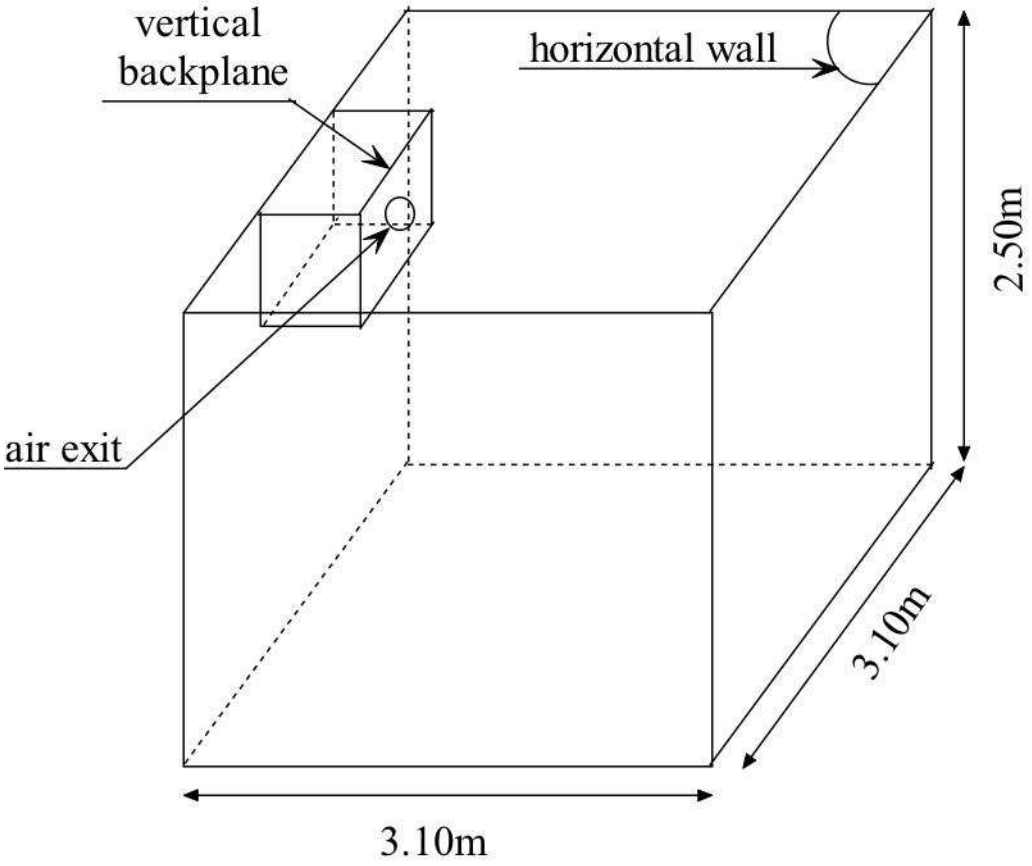

Figure 2 Schematic of the test room with geometry

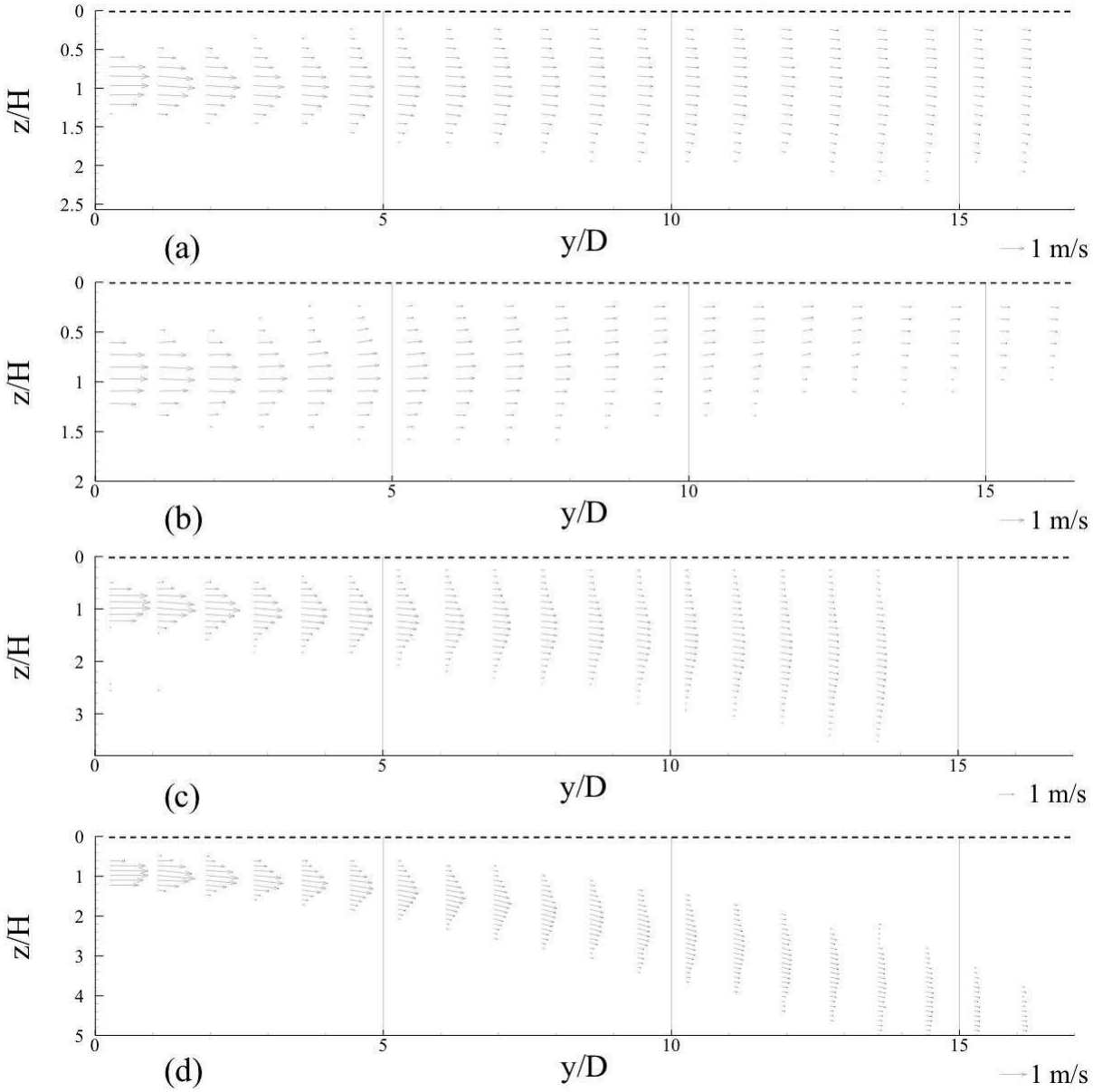

Figure 3 Mean velocity vector fields in the median plan for the cases I (a), H (b), C1 (c) and C2 (d)

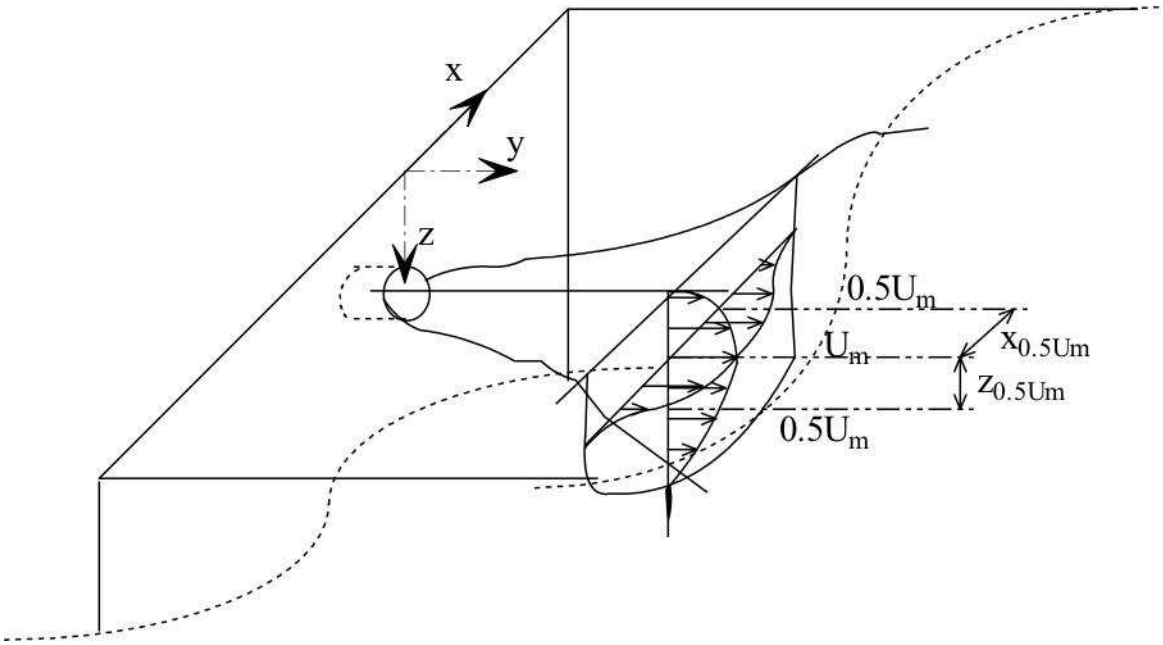

Figure 4 Schematic of the three-dimensional jet with coordinates

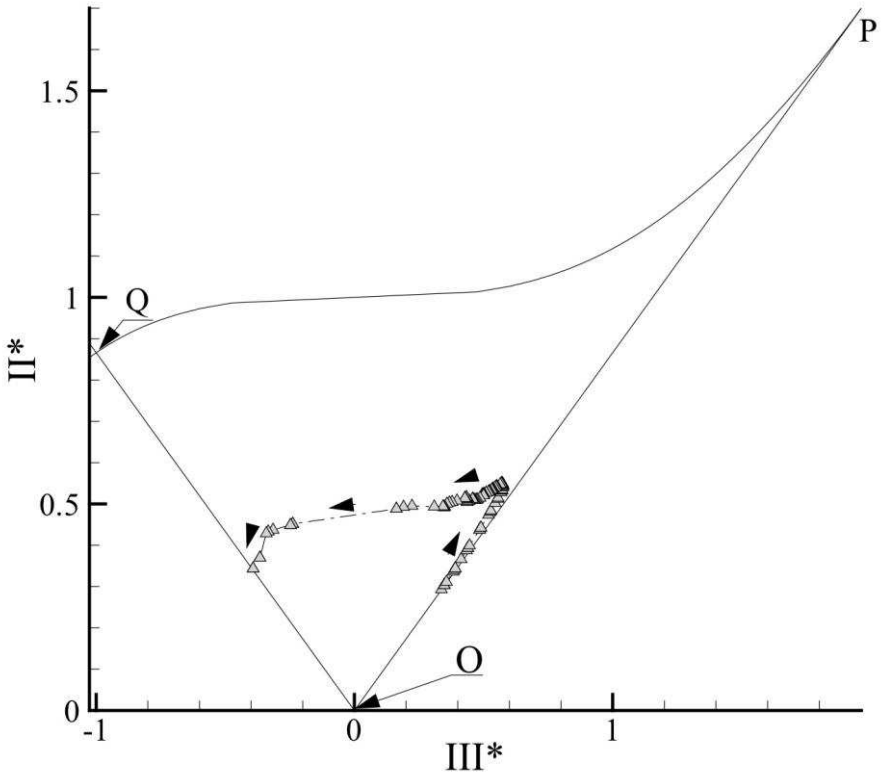

Figure 5 The Lumley triangle on the plane of the invariants II^* and III^* of the Reynolds-stress anisotropy tensor. The triangles correspond to values found by Hussein et al. (1994) in the axisymmetric zone of a free isothermal round jet at Re = 95500. The arrows show the increasing distance between the centerline of the jet and the point considered

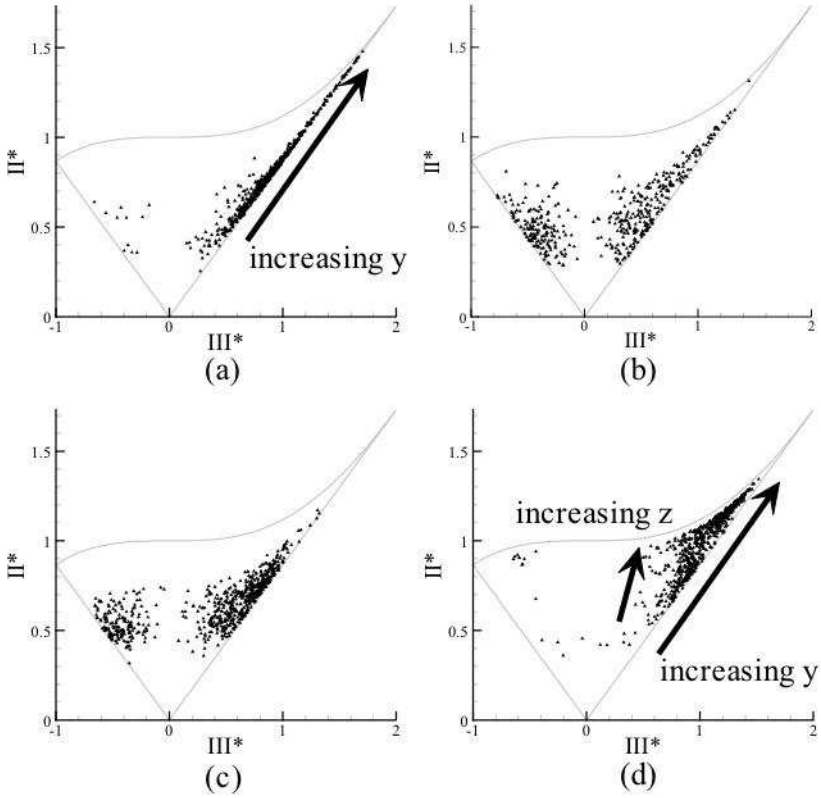

Figure 6 Lumley triangles for points in the median plan and for the cases I (a), H (b), C1 (c) and C2 (d)

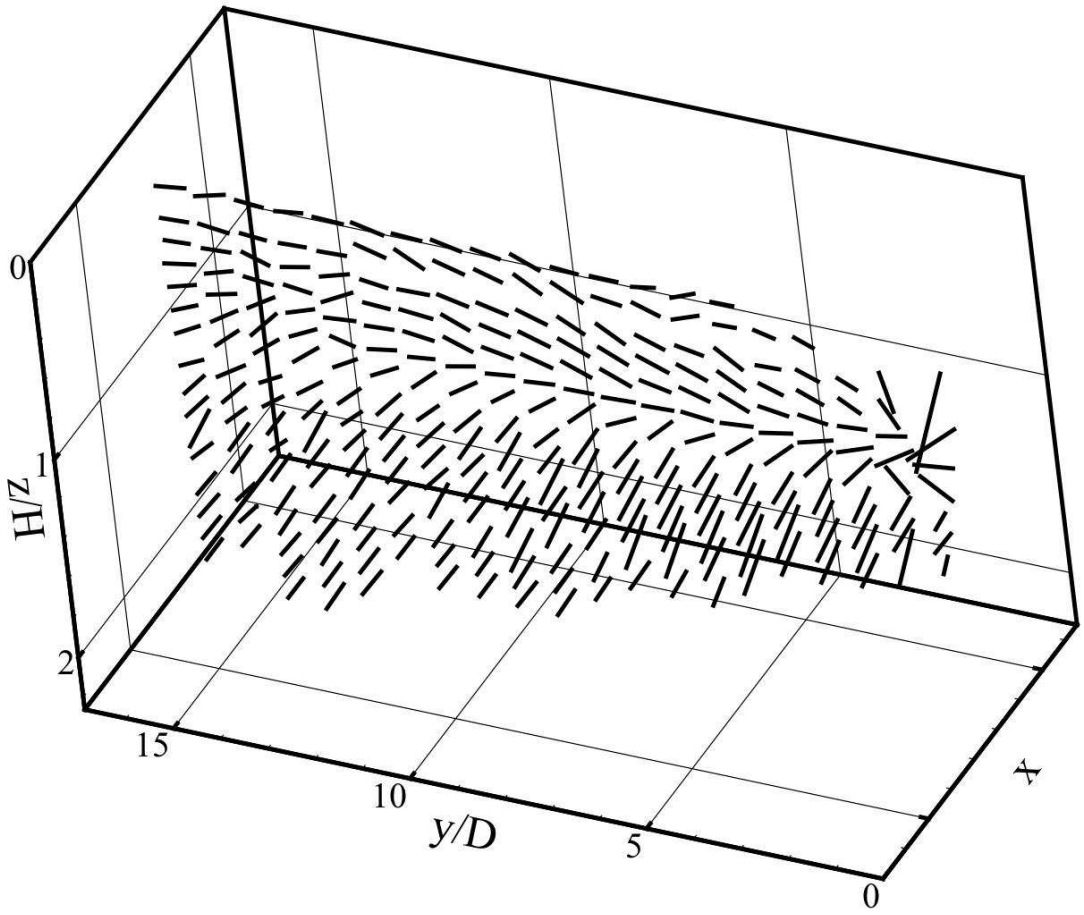

Figure 7 Directions of the eigenvectors associated to the highest eigenvalues of the Reynolds-stress tensor for some measurements points of the median plan - case I

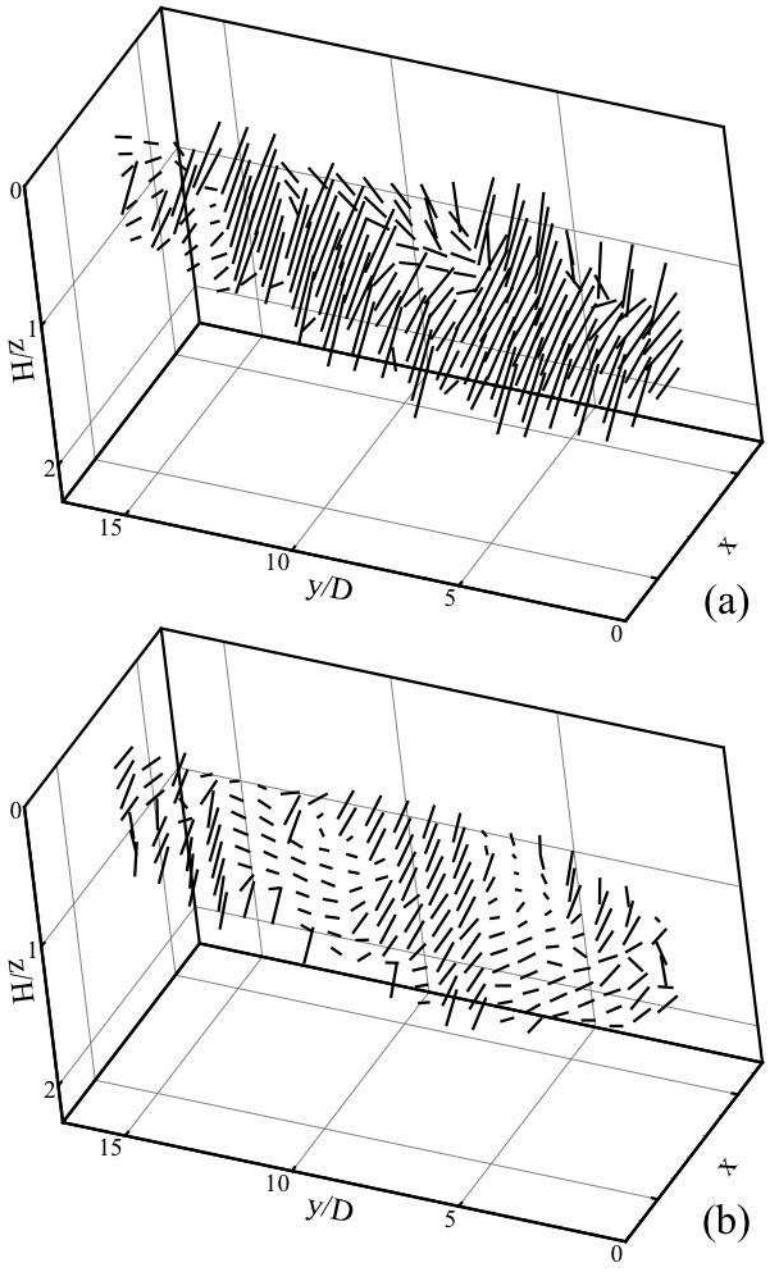

Figure 8 Directions of the eigenvectors associated to the highest eigenvalues (a) and the second highest eigenvalues (b) of the Reynolds-stress tensor for some measurements points of the median plan - case H

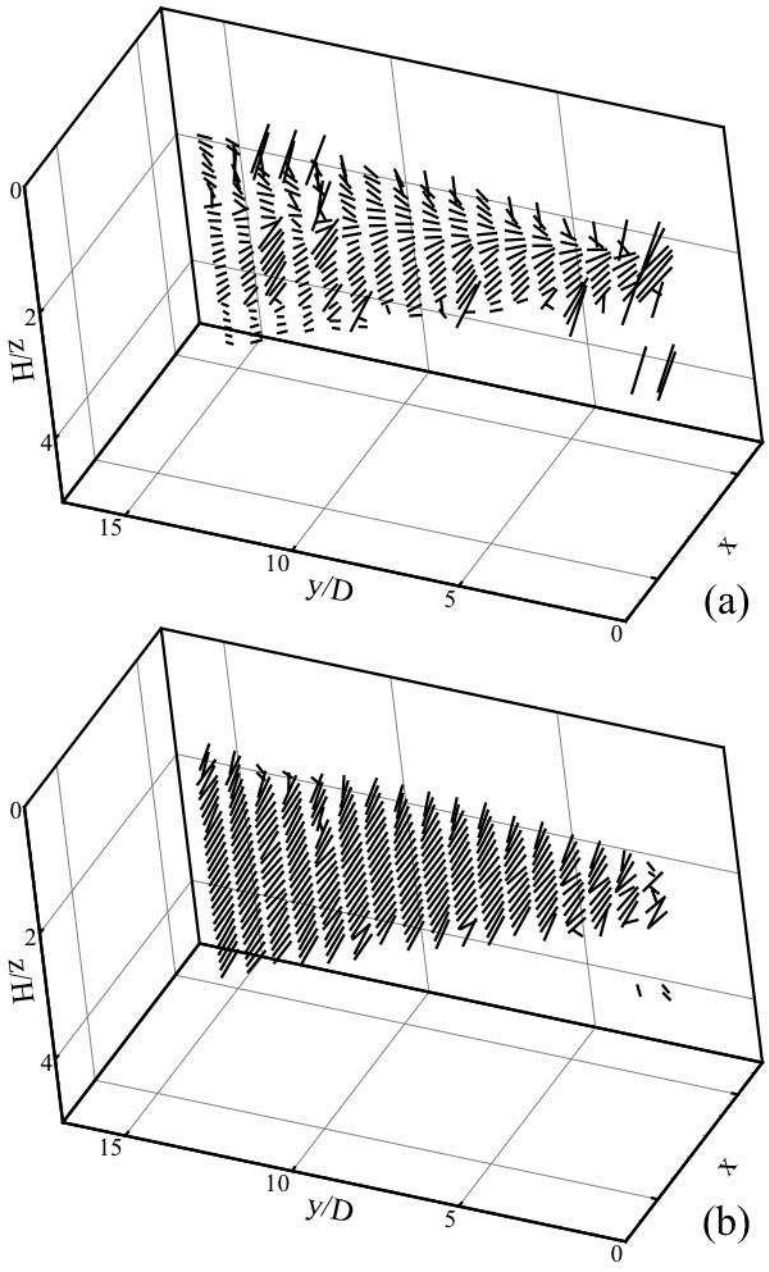

Figure 9 Directions of the eigenvectors associated to the highest eigenvalues (a) and the second highest eigenvalues (b) of the Reynolds-stress tensor for some measurements points of the median plan - case C1

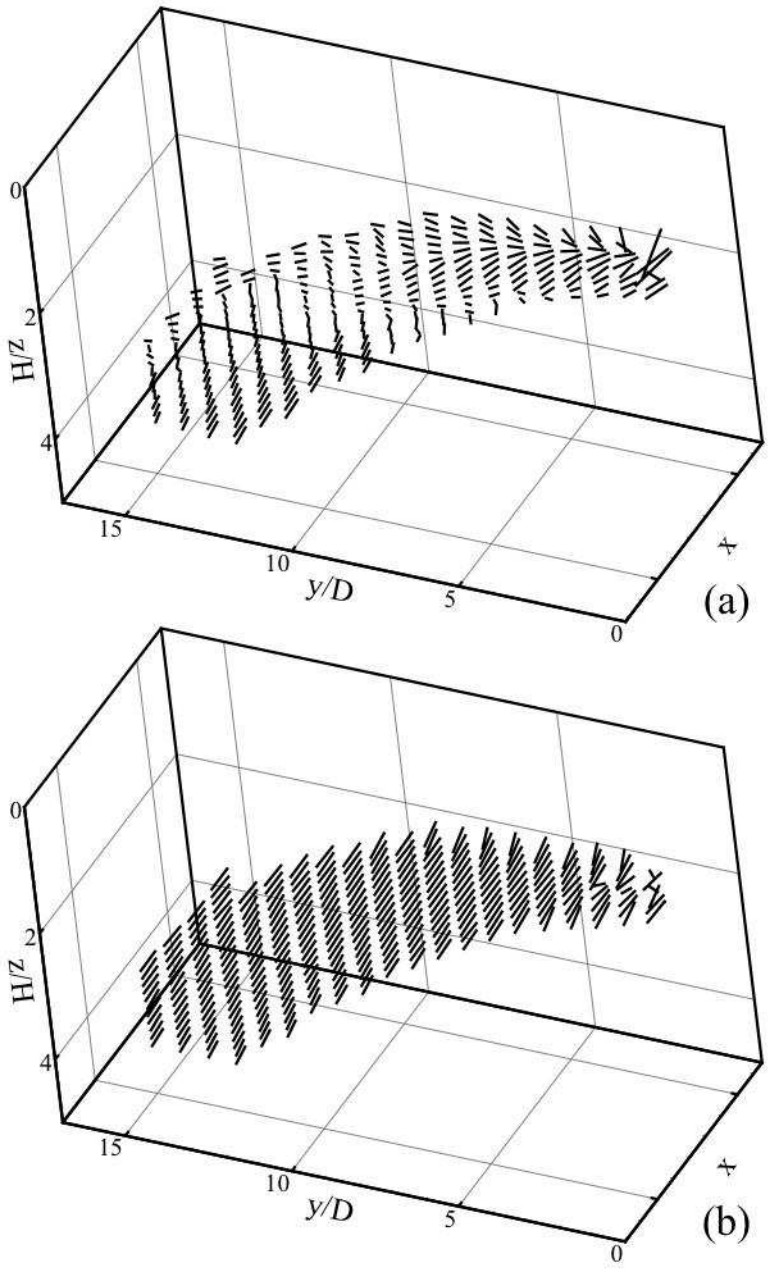

Figure 10 Directions of the eigenvectors associated to the highest eigenvalues (a) and the second highest eigenvalues (b) of the Reynolds-stress tensor for some measurements points of the median plan - case C2

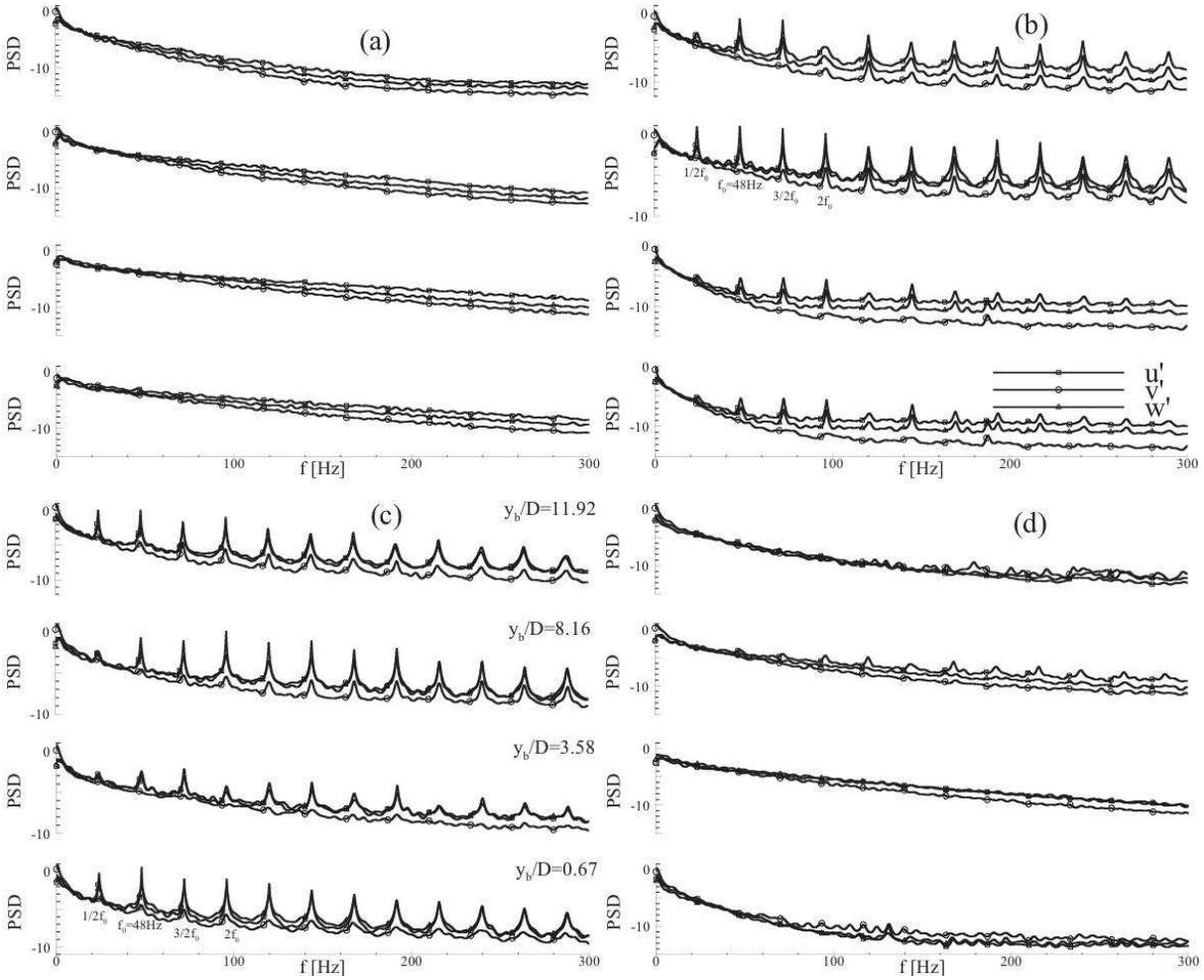

Figure 11 Power spectral density (arbitrary unit) for four points along y axis. The four cases presented are case I (a), case H (b), case C1 (c) and case C2 (d)

Table 1
Conditions during experimentations

	$Re_{0,d}$	$Ar_{0,d}$
Isothermal case I	13360	0
Hot case H	12800	0.0097
Cold case C1	20800	-0.0047
Cold case C2	11760	-0.014

Table 2
Jet expansion rates

	α_v	α_l	α_v/α_l
Isothermal case I	0.100	0.052	1.9
Hot case H	0.079	0.126	0.6
Cold case C1	0.100	0.011	0.9
Cold case C2	0.104	0.038	2.7

Table 3
States of the Reynolds-stress tensor in terms of the invariants II^* and III^* and the eigenvalues of R_{ij}

State of turbulence	Invariants	Eigenvalues of R_{ij}	Designation in figure 5
Isotropic	$II^* = III^* = 0$	$\lambda_1 = \lambda_2 = \lambda_3$	O
Two-component axisymmetric	$II^* = \frac{\sqrt{3}}{2}, III^* = -1$	$\lambda_1 = \lambda_2, \lambda_3 = 0$	Q
One-component	$II^* = \sqrt{3}, III^* = 2$	$\lambda_1 = \lambda_2 = 0$	P
Axisymmetric (one large eigenvalue)	$II^* = \frac{\sqrt{3}}{2} III^*$	$\lambda_1 = \lambda_2 < \lambda_3$	OP
Axisymmetric (one small eigenvalue)	$II^* = -\frac{\sqrt{3}}{2} III^*$	$\lambda_1 = \lambda_2 > \lambda_3$	OQ
Two-component	$II^* = -\sqrt{1 + \frac{1}{4} III^{*3}}$	$\lambda_1 = \lambda_2$	PQ
Prolate spheroid or cigar	$III^* > 0$	$\lambda_1 > \lambda_3, \lambda_2 > \lambda_3$	$III^* > 0$
Oblate spheroid or pancake	$III^* < 0$	$\lambda_1 < \lambda_3, \lambda_2 < \lambda_3$	$III^* < 0$